Available online at www.sciencedirect.com
ScienceDirect
Journal of Power Sources 167 (2007) 258–264
JOURNAL OF POWER SOURCES
www.elsevier.com/locate/jpowsour

Effect of starting particulate materials on microstructure and cathodic performance of nanoporous LSM–YSZ composite cathodes

Hwa Seob Song [a], Wi Hun Kim [a], Sang Hoon Hyun [a], Jooho Moon [a,*], Joosun Kim [b], Hae-Weon Lee [b]

[a] *Department of Materials Science and Engineering, Yonsei University, Seoul 120-749, Republic of Korea*
[b] *Nano-Materials Research Center, Korea Institute of Science and Technology, Seoul 136-791, Republic of Korea*

Received 30 October 2006; accepted 30 January 2007
Available online 1 March 2007

Abstract

Nano-scale LSM–YSZ composite electrodes are prepared from a mixture of yttria stabilized zirconia (YSZ) and strontium-doped lanthanum manganite (LSM) particles. Commercial YSZ particles are mixed with polymerizable complex method-driven LSM powders of two different particle sizes, namely, 81 and 210 nm. Then, the correlations between the properties of the starting particles, sintering temperature, microstructure and cell performance are studied. Use of smaller LSM particles in the composite electrode induces extensive grain growth. This significantly reduces the triple phase boundary (TPB) and leads to an increase in the polarization resistance. The composite cathode derived from larger LSM particles exhibits a lower total polarization resistance (∼0.31 Ω cm^2 at 800 °C) and, subsequently, better maximum cell power (∼630 mA cm^{-2}). By contrast, larger resistance and lower cell power are observed for electrodes composed of smaller LSM particles.

Keywords: Solid oxide fuel cell; Strontium-doped lanthanum manganite; Microstructure; Cathode; Yttria stabilized zirconia

1. Introduction

A solid oxide fuel cell (SOFC) is a device that converts the chemical energy of fuels directly to electricity through an electrochemical reaction of the fuels with an oxidant, typically oxygen from air. Conventional SOFCs are operated at high temperatures up to ∼1000 °C and are based on well-established component systems. Strontium-doped lanthanum manganite ($La_{1-x}Sr_xMnO_3$, LSM) is frequently utilized as a cathode material because of its high electrochemical activity for oxygen reduction and good stability and compatibility with yttria stabilized zirconia (YSZ) electrolyte. The use of LSM is inapplicable for a low-temperature SOFC, however, due to its low oxygen ion conductivity and high activation energy.

The addition of a YSZ component to the cathode of a SOFC is a general method to enhance the electrochemical performance of the LSM-based system. The addition of a highly ionic conductive YSZ phase to the LSM electrode layer is effective due to enlargement of the electrochemically active area, i.e., the triple phase boundary (TPB), at which the oxygen reduction reaction occurs. Accordingly, LSM–YSZ composite electrodes have demonstrated better performance than those composed of only LSM [1–4] since the TPB can extend three-dimensionally into the composite cathode. This means that the site density and spatial distribution of the TPB play a critical role in determining cell performance. The cathodic microstructure strongly influences the expansion of the TPB site density [5–7].

The electrode in the SOFC is fabricated from the ceramic particulate materials by sintering. The microstructure of the resulting electrode is governed by several processing parameters such as the size and distribution of the starting particle and the sintering conditions. In particular, the composite cathodes involve at least more than two different materials in which the constituents may differ in their densification behaviour. The use of nanoparticle-based cathode materials may allow enlargement of the TPB due to the increased particle-to-particle contact

* Corresponding author. Tel.: +82 2 2123 2855; fax: +82 2 365 5882.
E-mail address: jmoon@yonsei.ac.kr (J. Moon).

0378-7753/$ – see front matter © 2007 Elsevier B.V. All rights reserved.
doi:10.1016/j.jpowsour.2007.01.095

points. The difference in sinterabilities between the phases may, however, prevent the development of the three-dimensionally interconnected composite microstructure because of the premature excess sintering of a more easily sinterable phase. In such a case, the relative ratio of the particle sizes for the composite materials together with the sintering temperature should be well-controlled to optimize the cell performance. In the present study, the composite cathodes consist of nano-sized LSM and YSZ powders, which are known to have a distinct densification behaviour. A study is made of the correlations between the properties of the starting particles, sintering temperature, microstructure and cell performance.

2. Experimental

$La_{0.7}Sr_{0.3}MnO_3$ powders were prepared using a polymerizable complex method [8,9]. Each of the metal salts was dissolved in water. Then, ethylene glycol and citric acid were used as a polymerization and complexation agent, respectively. Polymerization occurred in the metallic salts solution upon heating. After polymerization, charring of the resin at 400 °C in air was performed before calcination at various temperatures to eliminate remaining organics and volatile species resulting from the polymeric resin, followed by calcination at 800 °C (denoted as *LSM800*) and 1000 °C (denoted as *LSM1000*) for 2 h. Transmission electron microscopic images of the synthesized particles are shown in Fig. 1. The mean particle size calculated from the specific surface area value is 81 nm for *LSM800* (surface area = 11.82 $m^2\ g^{-1}$) and 210 nm for *LSM1000* (surface area = 4.53 $m^2\ g^{-1}$).

LSM–YSZ composite materials were obtained by planetary milling of YSZ powder (Tosoh TZ8Y, surface area = 12.74 $m^2\ g^{-1}$, mean particle size = 78 nm) with two differently sized LSM powders in a weight ratio of LSM:YSZ = 6:4. The mixed composite cathodes were constructed by a screen-printing method with paste materials that were a mixture of the powders and additives dispersed in an organic solvent.

The paste of the composite cathode was placed on both sides of a 0.5 mm thick YSZ disc in a symmetrical cell configuration for the measurement of interfacial polarization resistance, and then a platinum mesh connected to a platinum wire was attached to the cathode layer for current-collection by means of platinum paste. The area of the applied cathode was 1.4 cm^2 and the thickness was 10–13 μm.

The NiO–YSZ substrate that had been prepared with liquid condensation precipitation (LCP) processed granules was used to measure cell performance [10,11]. A YSZ electrolyte of 14–15 μm in thickness was placed on the anode support via a dip-coating method [12]. One side of the support was polished to remove the YSZ electrolyte and to adjust the anode support thickness to ∼0.8 mm. All the YSZ/anode supports used for cell performance measurement were controlled to have the same dimensions so that any variation in the electric performance of the cells can be considered to originate solely from a difference in cathodic performance.

The sintering temperature for the composite cathode on top of the YSZ/anode supports was varied from 1100 to 1200 °C for 4 h. Four different LSM–YSZ layers were fabricated using different initial particles with different sintering temperatures. The microstructures of the resulting half- and full-cells were investigated by means of scanning electron microscopy (FE-SEM, JSM 6700F, JEOL). The densification behaviour of the cathode materials with different compositions during the heat treatment process was analyzed with a dilatometer (DIL402C, NETZSCH).

Electrochemical impedance measurements were performed on symmetrical cells, LSM–YSZ/YSZ/LSM–YSZ, with various oxygen partial pressure atmospheres using a Solatron SI 1260/1287 instrument. The impedance spectra were obtained over a frequency range from 100 kHz to 0.1 Hz with an applied ac voltage amplitude of 20 mV at temperatures from 600 to 850 °C in 50 °C intervals. Full-cell performance was investigated using a Solatron 1286 unit interfaced with a computer with humidified hydrogen as fuel and air as oxidant at ambient pressure and 800 °C.

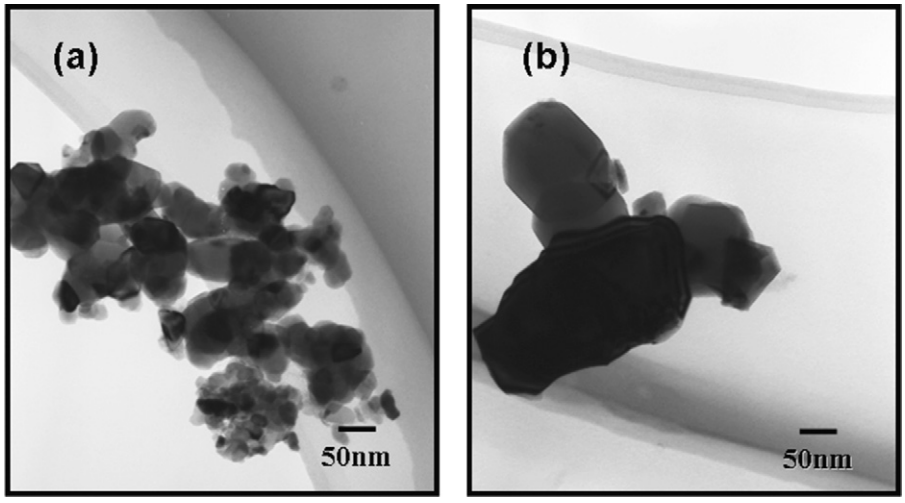

Fig. 1. TEM images of: (a) LSM800 and (b) LSM1000 particles.

3. Results and discussion

The total cathodic polarization resistances of the composite with different sized LSM particles are listed in Table 1. Interfacial resistances measured by ac impedance spectroscopy should be corrected for electrode area and divided by two in order to obtain area-specific polarization resistances in $\Omega\,cm^2$ [13]. The composite cathode consisting of a mixture of *LSM800* and YSZ sintered at 1100 °C for 4 h is denoted as *LSM800-YSZ@1100*. This sample exhibits the lowest resistance, whereas *LSM800-YSZ@1200* has the highest value. The resistances of

Table 1
Cathodic polarization resistance of half-cell using LSM800 and LSM1000 particles at 800 °C

Cathode type	Cathodic polarization resistance ($\Omega\,cm^2$)
LSM800-YSZ@1100	0.40
LSM800-YSZ@1200	0.73
LSM1000-YSZ@1100	0.31
LSM1000-YSZ@1200	0.51

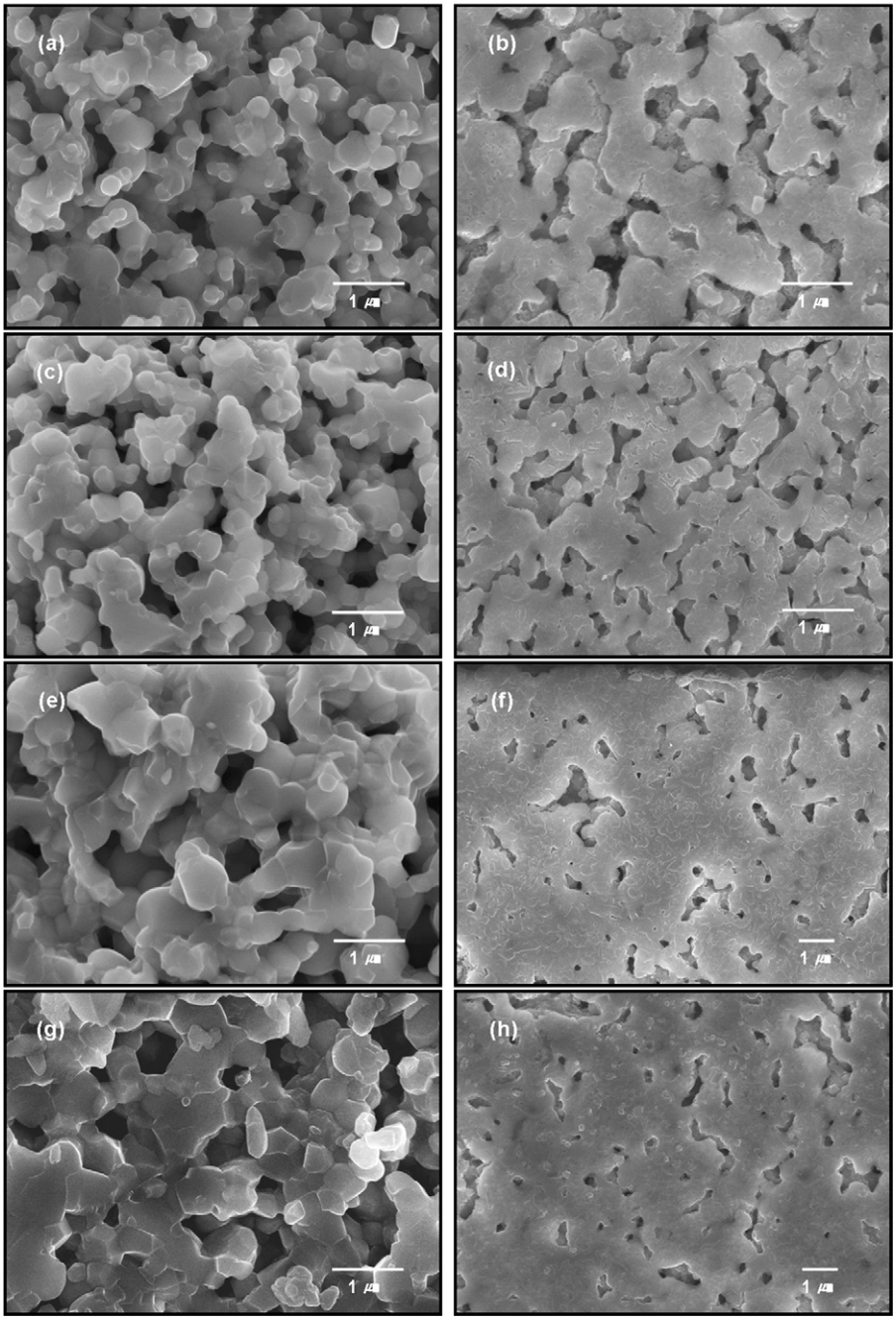

Fig. 2. SEM images of composite cathodes with different LSM particle sizes and sintering temperatures: (a) fractured and (b) polished images of LSM800-YSZ sintered at 1100 °C; (c) fractured and (d) polished images of LSM800-YSZ sintered at 1200 °C; (e) fractured and (f) polished images of LSM1000-YSZ sintered at 1100 °C; (g) fractured and (h) polished image of LSM1000-YSZ sintered at 1200 °C.

half-cells comprised of the same sized LSM particles increase with increasing sintering temperature. The cell prepared from the larger LSM particles (i.e., *LSM1000*) shows lower polarization resistance compared with that prepared from the smaller LSM (i.e., *LSM800*) when both are sintered at the same temperature. It is likely that the use of the smaller LSM particles allows more LSM–YSZ particle contact points and subsequently leads to a composite cathode with a larger number of TPB sites in which the LSM and YSZ phases are well-mixed as a three-dimensionally interpenetrated structure. Specifically, it is expected that *LSM800-YSZ@1100* will exhibit better cathodic properties than *LSM1000-YSZ@1100*; but the experimental results run counter to this expectation. Observation of the microstructures of the composite cathodes may provide an understanding of this discrepancy.

Fractured cross-sectional views of composite cathodes prepared with different particle sizes and sintering temperatures are presented in Fig. 2(a, c, e, and g). In general, the electrode sintered at 1100 °C exhibits a porous structure without significant densification compared with the electrode sintered at 1200 °C. In addition, the particles are well connected, not only with each other but also with the electrolyte layer at both temperatures. The influence of LSM particle size on the composite microstructure is, however, difficult to recognize from the fractured SEM images.

The samples were polished in order to achieve better microstructural analysis. The polished surfaces appear denser compared with the fractured ones, as shown in Fig. 2(b, d, f, and h). The microstructures of the electrodes are affected by both the LSM powder type and the sintering temperature. The samples with *LSM1000* and *LSM800* particles sintered at 1100 °C have porosities of approximately 40 and 37%, respectively, whereas 20 and 15% porosities are measured for the samples sintered at 1200 °C, as determined by image analysis. In addition, the cathode prepared from the *LSM1000* powder has slightly finer pores and smaller grains. Scanning electron microscopic analysis and even back-scattered electron images are unable to distinguish between the LSM and YSZ phases due to the nano-scale grain structures. These merely different microstructural features between the composite cathodes as a function of the particle sizes and sintering temperatures are insufficient to understand clearly the difference in cathodic performance. In this respect, a more detailed analysis is necessary.

To gain a better understanding of the relationship between electrochemical properties and cathode microstructural features, such as the TPB length and LSM/YSZ phase connectivity, the cathodic polarization resistances were measured as a function of the oxygen partial pressure. A typical impedance spectrum for a symmetrical cell, LSM–YSZ/YSZ/LSM–YSZ, measured at 750 °C under open-circuit conditions is given in Fig. 3(a). It is well-known that the impedance spectrum of a composite cathode is complex. In a Nyquist plot, the impedance is composed of a number of more or less overlapping arcs, each of which represents various electrode kinetic processes. Impedance analysis as a function of oxygen partial pressure enables each arc to be correlated to a specific electrode reaction mechanism. It has

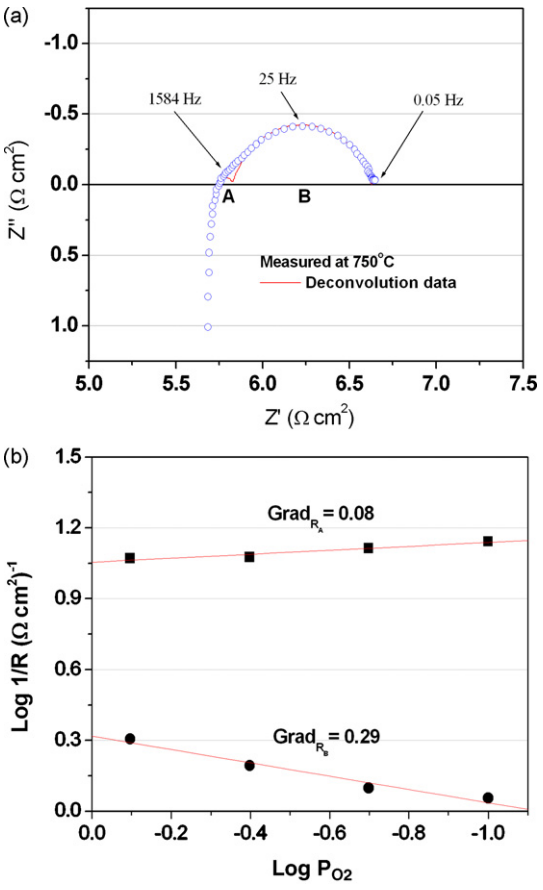

Fig. 3. (a) Typical impedance spectrum and deconvoluted arcs for symmetrical cell, LSM–YSZ/YSZ/LSM–YSZ, as measured at 750 °C in air under open-circuit conditions. (b) Plot of log $1/R$ vs. log P_{O_2} for composite cathode. R_A represents the high-frequency resistance, and R_B the low-frequency resistance.

been reported [14,15] that the impedance spectra of the cathodic half-cells can be divided into at least two different arcs that are denoted as process A (high frequency) and B (low frequency), as shown in Fig. 3(a). In the present study, the resistance of process A (R_A) is found to be always smaller than that of process B (R_B). The value of process A is also independent of the oxygen partial pressure. On the other hand, the magnitude of arc B is strongly dependent on the oxygen partial pressure. As shown in Fig. 3(b), the high-frequency A arc is nearly independent of P_{O_2}, whereas a $P_{O_2}^{-0.29}$ dependence is observed for the low-frequency B arc.

The distinct oxygen partial pressure dependence indicates that each arc represents a characteristic electrode process. Process A can be influenced by a transport of oxygen ions through either the YSZ or LSM|YSZ interface [14,16,17]. In other words, the magnitude of R_A relates to phase interconnectivity between either LSM and YSZ or YSZ and YSZ phases. Process B, characterized by a strong oxygen pressure dependence, is presumably associated with the charge-transfer process that occurs at the TPB and includes dissociative adsorption of the oxygen, surface diffusion of adsorbed species towards the TPB, and transfer to the oxygen ion as incorporated into the lattice. Thus, process B mainly reflects electrochemical oxygen reduction on the

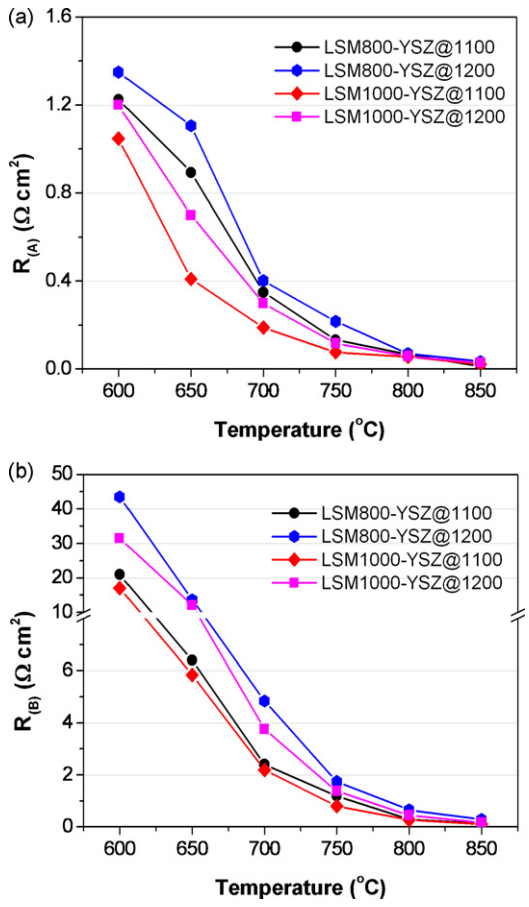

Fig. 4. Polarization resistance of (a) process A (R_A) and (b) process B (R_B). Impedance spectra obtained in air at 600–850 °C using symmetrical cell as function of cell operating temperature.

cathode, which is a strong function of the TPB site density [15,18].

The interfacial polarization resistances separated into the A and B processes for symmetrical cells with four different LSM–YSZ layers are presented in Fig. 4. The resistances increase with decreasing measurement temperature regardless of the half-cell type due to a reduction in oxygen conduction and catalytic activity. The difference in polarization resistance between the cells becomes clear when the impedance spectroscopy is measured in a low-temperature range (600–700 °C) as opposed to a high-temperature range (750–850 °C). All R_A values for the composite cathodes with *LSM800* are higher than those with *LSM1000*, as shown in Fig. 4(a). This indicates that the cathode layers composed of *LSM800* have relatively poorer phase interconnectivity than the cathodes with LSM1000. The R_A also increases with sintering temperature.

According to one of the possible reaction mechanisms, the oxygen gas is first adsorbed on the electrode surface and reduced at the TPB site to produce oxygen ions and consume electrons. The oxygen ions are then transported through the ionic transport pathway to the electrolyte. Adler et al. [19] have reported that the principal electrode polarization losses are usually associated with the generation and transport of oxygen ions within the porous cathode structure. Therefore, the ionic conduction pathway plays an important role in determining cathodic performance. On increasing the firing temperature, the YSZ phase begins to be sintered to form a three-dimensionally interconnected microstructure together with LSM. Under such conditions, both electronic and ionic transport pathways should build up throughout the electrode. The use of finer powders and higher sintering temperature degrades the phase interconnectivity in the composite cathode. Highly sinterable, finer, LSM particles undergo excess densification with increasing firing temperature, which adversely affects the contiguity between the phases and, in turn, prevents the formation of a sufficient ionic conduction pathway between either the LSM|YSZ or YSZ|YSZ interface. The influence of particle size and sintering temperature on electrode microstructure is well revealed by the R_A values.

The variation of polarization resistance of process B for the composite electrodes as a function of the starting LSM powder and sintering temperature is given in Fig. 4(b). The R_B values are larger than the R_A ones for all the measured samples. Thus, the total polarization resistance depends on R_B. The lowest value of the polarization resistance is 0.26 Ω cm^2 for *LSM1000-YSZ@1100*, whereas the *LSM800-YSZ@1200* sample has a resistance of 0.66 Ω cm^2. Higher R_B values are found for the cells sintered at 1200 °C than for those sintered at 1100 °C. This implies that sintering at 1200 °C makes the electrode denser, which decreases the TPB site density, and that the proper sintering temperature for the composite cathode is 1100 °C. At the same firing temperature, the composite cathode from *LSM1000* shows a smaller R_B value than that from *LSM800*. This clearly indicates that a greater TPB site density is associated with the composite electrode from *LSM1000*. It is believed that excess densification by finer LSM particles prevents the cathode from forming sufficient TPB sites, and thereby increases the polarization resistance.

The shrinkage behaviour of the various cathode materials tested in the form of bar-shaped specimens during the sintering process is shown in Fig. 5. As expected, the densification for *LSM800* starts at a much lower temperature than that for

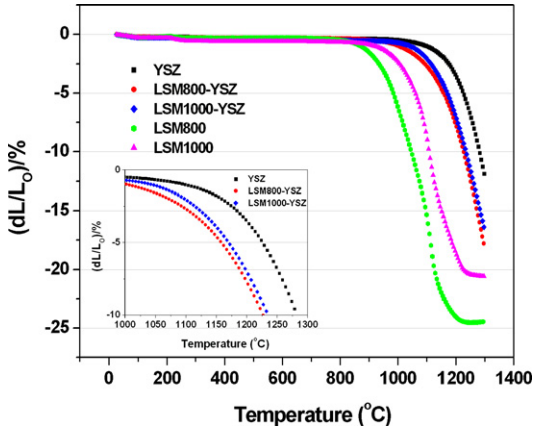

Fig. 5. Shrinkage behaviour for various cathode samples heated to 1300 °C.

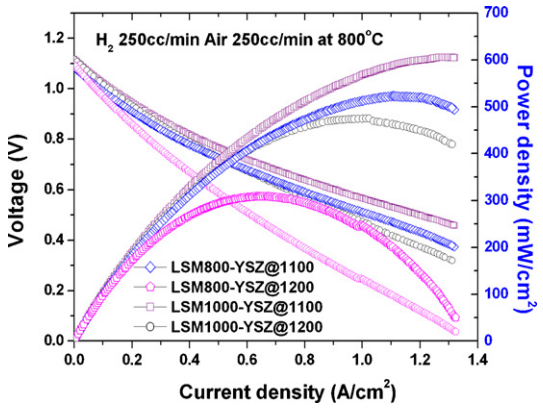

Fig. 6. Cell performances for fuel cells incorporating various composite cathodes.

LSM1000, *LSM800* and *LSM1000* particles began to densify at about 850 and 920 °C, respectively. Noticeable shrinkage of the YSZ phase occurs near 1100 °C. On the other hand, the LSM–YSZ composite materials undergo volumetric shrinkage at around 1000–1050 °C. The addition of YSZ prevents to some extent the oversintering of the LSM phases, but its effectiveness deteriorates as the LSM particle size decreases. The LSM800-YSZ cathodes shrink more than 30% at 1100 °C and 10% at 1200 °C as compared with the LSM1000-YSZ cathode. Analysis of the shrinkage behaviour supports the conclusion that excess densification of more sinterable *LSM800* particles inhibits the YSZ-to-YSZ phase connection and reduces the TPB site density. Further, the findings suggest that an optimum particle size ratio exists between the LSM and YSZ to produce a desirable electrode microstructure. The more easily sinterable LSM phase should have a larger particle size than YSZ. Under the present experimental conditions, the mean particle size ratio of LSM800/YSZ and LSM1000/YSZ is ∼1 and 2.7, respectively. The optimum particle size ratio should also vary according to the value of the particle size. The optimum particle size ratio will be larger as coarser YSZ particles larger than 78 nm are used.

The full-cell performance of LSM–YSZ/YSZ/Ni–YSZ cells with different composite cathodes was investigated using a humidified hydrogen. To distinguish the influence of the composite cathodes on the cell power performance, the electrolyte and anode thicknesses are identical for the four different cells. The discharge profiles of the cells at 800 °C are presented in Fig. 6. The open-circuit voltage (OCV) of the tested cells is about 1.1 V. The four different cells exhibit the same order of cell power performance as the corresponding cathodic performances, as shown in Table 1. A maximum power density of ∼630 mW cm^{-2} is observed at a current density of 1.3 A cm^{-2} for the cell with a *LSM1000-YSZ@1100* composite cathode of 0.31 Ω cm^2. On the other hand, the cell with a *LSM800-YSZ@1200* composite cathode of 0.73 Ω cm^2 delivers only ∼305 mW cm^{-2}. The maximum cell power is almost inversely proportional to the total cathodic polarization resistance. These observations clearly demonstrate that the cathodic electrochemical performance closely correlates with the microstructural features, which are strongly influenced by the starting particle characteristics and processing conditions.

4. Conclusions

An investigation has been undertaken of the correlation between electrochemical performance and the microstructure of SOFC cathodes consisting of a submicron-sized composite LSM–YSZ. Impedance spectroscopy analysis as a function of the oxygen partial pressure provides a better understanding of the variation in polarization resistance as a function of sintering temperature and starting particle size in terms of cathode microstructural features, which are hardly evaluated by SEM when the LSM–YSZ composite has a nano-scale grain structure. The more sinterable nano-sized LSM particles undergo excess grain growth so as to inhibit TPB formation and ionic conduction pathways, which impairs both the cathodic electrochemical and cell performances. For better electrochemical performance, the LSM and YSZ particle sizes and subsequent processing conditions have to be well-controlled for the composite cathode to have three-dimensionally well-interconnected structures with a maximum TPB site density.

Acknowledgements

This work was supported by the Core Technology Development Program for the Fuel Cell of Ministry of Commerce, Industry, and Energy and the Korea Institute of Science and Technology Evaluation and Planning. It was also partially supported by the Korea Science and Engineering Foundation (KOSEF) through the National Research Lab. Program funded by the Ministry of Science and Technology (No. M10500000011).

References

[1] T. Tasi, S.A. Barnett, Solid State Ionics 93 (1997) 207–219.
[2] E.P. Murry, S.A. Barnett, Solid State Ionics 143 (2001) 265–273.
[3] T. Kenjo, M. Nishiya, Solid State Ionics 57 (1992) 295–302.
[4] M.J.L. Østergard, C. Clausen, C. Bagger, M. Mogensen, Electrochim. Acta 40 (12) (1995) 1971–1981.
[5] K. Sasaki, J.-P. Wurth, R. Gschwend, M. Godickemeier, L.J. Gauckler, J. Electrochem. Soc. 143 (2) (1996) 530–543.
[6] F. van Heuveln, H.J.M. Bouwmeester, F.P.F. van Berkel, J. Electrochem. Soc. 144 (1) (1997) 126–133.
[7] M.J. Jorgensen, S. Primdahl, C. Bagger, M. Mogensen, Solid State Ionics 139 (2001) 1–11.
[8] M. Popa, J. Frantti, M. Kakihana, Solid State Ionics 154–155 (2002) 437–445.
[9] M. Kakihana, M. Arima, M. Yoshimura, N. Ikeda, Y. Sugitani, J. Alloys Compd. 283 (1999) 102–105.
[10] H. Lunhleich, J. Dias, H. Nickel, Carbon 35 (1) (1997) 95–102.
[11] D.-S. Lee, J.-H. Lee, J. Kim, H.-W. Lee, H.S. Song, Solid State Ionics 166 (2004) 13–17.
[12] S.D. Kim, S.H. Hyun, J.M. Moon, J.-H. Kim, R.H. Song, J. Power Sources 139 (2005) 67–72.
[13] C. Xia, Y. Zhang, M. Liu, Electrochem. Solid-State Lett. 6 (2003) A290–A292.

[14] M.J. Jorgensen, M. Mogensen, J. Electrochem. Soc. 148 (2001) A433–A442.
[15] M. Juhl, S. Primdahl, M. Mogensen, in: F.W. Poulsen, N. Bonanos, S. Linderoth, M. Mogensen, B. Zachau-Christiansen (Eds.), High Temperature Electrochemistry: Ceramics and Metals, Risø National Laboratory, Denmark, 1996, pp. 295–301.
[16] E.M. Skou, T. Jacobsen, Appl. Phys. A 49 (1989) 117–121.
[17] J. Fleig, P. Pham, P. Sztulzaft, J. Maier, Solid State Ionics 113–115 (1998) 739–747.
[18] M.J.L. Østergard, M. Mogensen, Electrochim. Acta 38 (14) (1993) 2015–2020.
[19] S.B. Adler, J.A. Lane, B.C.H. Steele, J. Electrochem. Soc. 143 (11) (1996) 3554–3564.